DRP1 regulates endoplasmic reticulum sheets to control mitochondrial DNA replication and segregation

Hema Saranya Ilamathi[1,2,3], Sara Benhammouda[1,2,3], Justine Desrochers-Goyette[1,2,3], Matthew A. Lines[4], Marc Germain[1,2,3#]

[1]Groupe de Recherche en Signalisation Cellulaire and Département de Biologie Médicale, Université du Québec à Trois-Rivières, Trois-Rivières, Québec, Canada

[2]Centre d'Excellence en Recherche sur les Maladies Orphelines - Fondation Courtois, Université du Québec à Montréal, Montréal, Québec, Canada

[3]Réseau Intersectoriel de Recherche en Santé de l'Université du Québec (RISUQ)

[4]Department of Medical Genetics, Cumming School of Medicine, University of Calgary, Calgary, Alberta, Canada

 # Correspondence: Marc Germain (marc.germain1@uqtr.ca)

Abstract

Mitochondria are multi-faceted organelles crucial for cellular homeostasis that contain their own genome. Mitochondrial DNA (mtDNA) codes for several essential components of the electron transport chain, and mtDNA maintenance defects lead to mitochondrial diseases. mtDNA replication occurs at endoplasmic reticulum (ER)-mitochondria contact sites and is regulated by mitochondrial dynamics. Specifically, mitochondrial fusion is essential for mtDNA maintenance. In contrast, while loss of mitochondrial fission causes the aggregation of nucleoids (mtDNA-protein complexes), its role in nucleoid distribution remains unclear. Here, we show that the mitochondrial fission protein DRP1 regulates nucleoid segregation by altering ER sheets, the ER structure associated with protein synthesis. Specifically, DRP1 loss or mutation leads to altered ER sheets that physically interact with mitobulbs, mitochondrial structures containing aggregated nucleoids. Importantly, nucleoid distribution and mtDNA replication were rescued by expressing the ER sheet protein CLIMP63. Thus, our work identifies a novel mechanism by which DRP1 regulates mtDNA replication and distribution.

Keywords: mtDNA, DRP1, fission, ER sheets, CLIMP63, mitochondria

Introduction

Mitochondria are dynamic organelles regulating an array of cellular processes including energy production, cellular metabolism, apoptosis, calcium signaling, ROS signaling, cellular differentiation and immune response against pathogens (*1-6*). These mitochondrial functions are regulated by mitochondrial dynamics, the processes of mitochondrial fusion and fission. Mitochondrial fission requires DRP1 (Dynamin-Related Protein 1) (*7, 8*), while fusion is regulated by Mitofusins 1 and 2 (MFN1 & 2) and Optic Atrophy Protein 1 (OPA1) present on mitochondrial outer and inner membrane respectively (*9, 10*). Mitochondrial dynamics are also essential for mitochondrial DNA (mtDNA) maintenance, with defects in mitochondrial fusion affecting mtDNA integrity and copy number (*11, 12*). On the other hand, while defective mitochondrial fission does not generally affect overall mtDNA content, it alters the distribution of nucleoids (mtDNA-protein packaging), leading to the formation of bulb-like mitochondrial structures termed mitobulbs (*13-16*). Importantly, both mitochondrial fission and mtDNA replication are initiated at sites of contact between mitochondria and the endoplasmic reticulum (ERMCS)(*17-19*), indicating a crucial role for the ER in the regulation of mitochondrial structure and function.

The ER is a complex web-like organelle that includes flattened cisternae/sheets around the perinuclear region and tubulated structures towards the cellular periphery (*20*). ER sheets/ rough ER (rER) are enriched with ribosomes and regulate the production and assembly of proteins for secretion (*21*). On the other hand, ER tubules / smooth ER (sER) play important roles in lipid synthesis and calcium signaling, but also mitochondrial dynamics and mtDNA replication (*17-19, 21*). At the molecular level, the ER resident protein CLIMP63 (CKAP4) is essential for the maintenance of ER sheets, while reticulons (RTN) and DP1/Yop1p are essential for both ER tubule formation and the maintenance of ER sheet curvature (*22, 23*). The ratio of sheet to tubule proteins regulates the balance between the two ER structures (*22*). In addition, recent studies showed that the mitochondrial fission protein DRP1 associates with the ER independently of mitochondria where it helps regulate ER tubulation (*24, 25*). While this suggests a complex interplay between mitochondria-shaping proteins and ER tubules, the role of ER sheets in these processes remains poorly understood. This is an important question because some reports suggest that ER sheets also contact mitochondria (*26*).

Here, we show that DRP1 controls the interaction between ER sheets and mitochondria by regulating ER sheet structure. Specifically, primary human fibroblasts from patients with a mutation in DRP1 showed altered ER sheet structure and increased interaction with mitochondria that were associated with a reduction in mtDNA replication and distribution. Importantly, modulating ER sheets through the expression of CLIMP63 rescued mtDNA replication and distribution in DRP1 mutants. Altogether, our results demonstrate that DRP1-dependent ER sheet dynamics regulates replication and distribution of mtDNA independently of mitochondrial dynamics.

Results

Mutation or knockdown of DRP1 alters ER sheet structure

DRP1 is a cytosolic protein that is recruited to mitochondria to cause mitochondrial fission (*27*). However, recent studies suggest that DRP1 associates with the ER prior to its transfer to mitochondria during mitochondrial fission (*24*). In addition to regulating mitochondrial dynamics, ER-localised DRP1 has been shown to regulate ER tubule formation independently of ER shaping proteins (CLIMP63, RTN4) (*25*). However, whether DRP1 also regulates ER sheets, the structure adopted by perinuclear ER, and potential effects on ER sheets-mitochondria interactions remain unclear. To address these questions, we measured the association of DRP1 with ER sheets in primary human fibroblasts. We marked cells for mitochondria (mitotracker orange), ER sheets (endogenous CLIMP63), and endogenous DRP1 and imaged them by confocal microscopy. While numerous DRP1 foci were observed along mitochondrial tubules (Fig 1A, arrows in left panel, line scan in right panel; Sup. Fig. 1A for the full image), we observed a sub-population of DRP1 associated with ER sheets independently of mitochondria (Fig 1A, arrowheads in left panel). Line scans of the images also revealed a distinct colocalization between DRP1 and CLIMP63 (Fig. 1A, right panel).

Given that DRP1 associates with ER sheets, we then determined the effect of DRP1 mutation on ER sheets. For this, we used primary fibroblasts from patients with a dominant-negative mutation in the middle domain of DRP1 which is required for DRP1 oligomerisation but not for its ER tubulation activity (*25, 28*). Control and DRP1 mutant patient fibroblasts were immunolabelled for ER sheets (CLIMP63) and imaged by confocal microscopy (Fig 1B). We manually classified cells based on their ER sheet features (structured or altered) and found that DRP1 mutants had disorganized ER sheets compared to control cells, with thick patches of sheets in the perinuclear region and a punctate appearance towards the periphery (Fig 1B-C). The area covered by ER sheets was also expanded in DRP1 mutant fibroblast (Fig. 1D). Nevertheless, protein levels of CLIMP63, RTN4, the general ER marker Calnexin and the mitochondrial proteins TOM20 and ATP5a were similar between control and DRP1 mutant cells, indicating that the changes induced by DRP1 mutation are not caused by changes in protein expression levels (Fig. S1C).

While our results suggest that DRP1 regulates ER sheet structure, we wanted to eliminate the possibility of secondary effects in the human DRP1 mutants we used. We thus knocked down DRP1 (DRP1 KD) in mouse embryonic fibroblasts (MEFs) (Fig S1B) and labelled them with CLIMP63 (ER sheets). Like patient fibroblasts, DRP1 KD MEFs had mostly punctate ER sheets (Fig 1E-F) that covered an expanded area of the cell (Fig 1G). On the other hand, neither DRP1 mutants nor DRP1 KD MEFs showed clear changes in ER tubules labelled with RTN4 (Fig S1D-E).

To further confirm the structural alteration in ER sheets, we imaged control and DRP1 mutant fibroblasts by transmission electron microscope (TEM) (Fig. 2A), where ER sheets are identified as rER. ER sheets from DRP1 mutants were short with less surface area and narrower luminal width compared to control ER sheets (Fig 2B-C), supporting our immunofluorescence data. On the other hand, ER tubule area and luminal width (identified as sER) were similar in control and DRP1 mutants (Fig 2D-E). Altogether, our data suggest that DRP1 associates with and modulates ER sheet structure.

Mutation in DRP1 affects ER sheets-mitochondria interaction

ER tubules interact with mitochondria to regulate mitochondrial dynamics (fusion and fission) and mitochondrial DNA replication (*17, 19*). On the other hand, putative contact sites between mitochondria and ER sheets have not been thoroughly characterised. As our results and recent work in mouse liver cells suggests that ER sheets functionally interact with mitochondria (*26*), we directly measured mitochondria-ER sheet contact sites using a proximity ligation assay (PLA) for CLIMP63 (ER sheets) and TOM20 (mitochondria). To assess the specificity of the interaction, we also co-labelled the cells for CLIMP63 and TOM20. Clear PLA foci were present at sites where CLIMP63 and TOM20 signals overlapped (Fig 3A, IgG control in Sup. Fig 2A), suggesting that ER sheets interact with mitochondria (Fig 3A, Zoom image). We specifically measured this interaction by manually counting PLA foci at the sites where CLIMP63 and TOM20 signals overlapped (Fig 3A-B). We then measured mitochondria-ER sheet interactions in DRP1 mutants. As shown in Fig 3A-B, DRP1 mutation significantly increased the interaction between mitochondria and ER sheets. A similar increase in PLA was also observed for the more general ER marker, Calnexin (Fig 3C, S2B), further suggesting that DRP1 regulates the interaction between the two organelles.

To further confirm our results, we imaged control and patient fibroblasts by TEM (Fig 3D) and manually quantified the interaction between ER sheets and mitochondria (≤30 nm) near the perinuclear region. We observed that mitochondria closely interacted with ER sheets in control fibroblasts. Consistent with the PLA data, this interaction was further enhanced in DRP1 mutant fibroblasts, as shown by the increase in both the number of ERMCS per mitochondrial length and the length of these ERMCS (Fig 3D-F). Altogether, our data indicates that ER sheets interact with mitochondria and that DRP1-dependent ER sheet structural changes alters this interaction.

ER sheets are associated with mitobulbs in DRP1 mutants

Loss of DRP1 results in mitochondrial elongation with the formation of bulb-like mitochondrial structures containing enlarged nucleoids (mitobulbs)(*13, 15, 16*). We observed a similar phenotype in DRP1 mutant fibroblasts stained for mitochondria (TMRM) and nucleoids (picogreen) and imaged by confocal microscopy (Fig 4A).

Given that, similar to ER sheets, mitobulbs are present in the perinuclear region of DRP1 mutant cells (*14*) and that ER sheets interact with mitochondria (Fig. 3), we hypothesized that ER sheet alterations in DRP1 mutants is associated with mitobulb formation. To test this, we analysed the interaction between ER sheets and mitobulbs. We first immunolabelled primary fibroblasts with CLIMP63 (ER sheets) and ATP5a (mitochondria) and imaged by confocal microscopy (Fig 4B). Line scan analysis showed that mitobulbs are in close association with ER sheets in DRP1 mutants. (Fig 4B-C). Further, we manually quantified the number of mitobulbs in close association with ER sheets. We found that the vast majority of mitobulbs are in close proximity to ER sheets (Fig 4D), supporting the idea that ER sheets interact with mitobulbs. To further confirm the presence of a physical interaction between mitobulbs and ER sheets, we performed PLA for CLIMP63 (ER sheets) and TOM20 (mitochondria). PLA foci were clearly visible at sites where ER sheets were in close proximity to mitobulbs (Fig 4E, quantification in F), consistent with an interaction between the two structures. Similar results were observed when Calnexin was used instead of CLIMP63 for the PLA (Fig 4F, S2C). Altogether, our results indicate that the altered ER sheets present in DRP1 mutants interact with mitobulbs.

Modulation of ER sheets recovers the nucleoid defects present in DRP1 mutants

To directly determine whether ER sheets affect nucleoid distribution, we modulated ER sheet structure by expressing mCherry-tagged CLIMP63 under conditions that did not overtly alter RTN4-positive ER tubules in control cells (Fig S3A) to avoid nucleoid defects caused by the loss of ER tubules (*19*). Importantly, CLIMP63 expression did not rescue the fused mitochondrial phenotype of DRP1 mutant (Fig. S3B). Nevertheless, CLIMP63 expression altered ER sheet structure resulting in expanded web-like ER sheet network in both control and DRP1 mutant fibroblasts (Fig S4). Importantly, this was accompanied by a loss of the punctate structures typically observed in mutant cells transfected with mCherry alone (Fig S4), suggesting that CLIMP63 expression can at least partially rescue the ER sheet defects observed in DRP1 mutants. To determine if this was associated with a change in ER sheets-mitochondria interactions, we performed PLA for CLIMP63 (ER sheets) and TOM20 (mitochondria). CLIMP63 expression did not affect mitochondria-ER sheet interaction in control cells (Fig 5A) but rescued the excessive contact sites found in DRP1 mutant cells (Fig. 5A). Similarly, the number of mitobulbs associated with PLA foci was reduced in DRP1 mutant cells expressing CLIMP63 (Fig. 5B), indicating that recovery of ER sheet structure in DRP1 mutants normalizes its interaction with mitochondria.

Loss of DRP1 results in enlarged nucleoids (Fig. 5C) that are likely caused by nucleoid aggregation (*14-16*). To confirm the presence of multiple mtDNA copies in the enlarged nucleoids present within mitobulbs, we labelled dividing nucleoids with the nucleotide analogue EdU and observed multiple EdU-positive foci within mitobulbs (Fig. 5D-E). To determine the effect of modulating ER sheets on this nucleoid aggregation, we transiently transfected control and DRP1 mutant fibroblasts with mCherry or mCherry-CLIMP63 and immunolabelled them for mitochondria (TOM20) and nucleoids (TFAM) (Fig S5). We first determined the effect of mCherry-CLIMP63 expression on nucleoid aggregation by measuring nucleoid size. Nucleoid size was significantly reduced in DRP1 mutants expressing mCherry-CLIMP63 compared to cells expressing only mCherry (Fig 5C, Fig. S5), consistent with CLIMP63 expression stimulating nucleoid distribution out of mitobulbs. We then reasoned that if CLIMP63 rescues nucleoid distribution, it should also rescue the decreased nucleoid numbers present in DRP1 mutant cells (Fig. 5F)(*14*). Indeed, while mCherry-CLIMP63 expression did not significantly affect nucleoid numbers in controls cells, it caused a significant increase in overall nucleoid content in DRP1 mutants (Fig 5F, Fig. S5). Altogether, these results indicate that modulating ER sheet structure can rescue nucleoid aggregation in DRP1 mutants. As the enlarged nucleoids present in DRP1 mutant cells are found within mitobulbs, we also determined the effect of mCherry-CLIMP63 expression on the presence of mitobulbs. While almost all mitobulbs present in mCherry-transfected DRP1 mutant fibroblasts contained TFAM-positive nucleoids, mCherry-CLIMP63 expression drastically reduced this number (Fig 5G). On the other hand, the total number of enlarged, bulb-like mitochondrial structures was unchanged (Fig 5H), suggesting that DRP1 is still required to maintain mitochondrial structure in these conditions. Altogether, our data indicates that ER sheets regulate nucleoid segregation in a DRP1-dependent manner, but independently of changes in mitochondrial structure.

Altering ER sheets in DRP1 mutant promotes mtDNA replication and distribution

While our results are consistent with CLIMP63 expression promoting nucleoid distribution away from mitobulbs, it remained possible that it also altered mtDNA replication. Thus, we measured the effect of CLIMP63 expression on mtDNA replication. Replicating DNA was labelled with

EdU, after which cells were directly fixed, immunolabelled for mitochondria (TOM20) and imaged by confocal microscopy. In cells expressing mCherry, DRP1 mutants had fewer EdU-positive nucleoids compared to control cells (Fig 6A), suggesting that DRP1 is required for proper mtDNA replication. Importantly, expression of CLIMP63 rescued the number of EdU foci in DRP1 mutant cells (Fig 6A), suggesting that the effect of DRP1 on nucleoid replication depends on its ability to modulate ER structure. On the other hand, CLIMP63 expression did not significantly alter the number of EdU foci in control cells (Fig 6A), indicating that modulating ER sheets does not directly affect mtDNA replication.

As clusters of EdU-positive mtDNA are found within mitobulbs (Fig. 5D-E), we then specifically addressed the effect of CLIMP63 expression on mtDNA replication within mitobulbs. Consistent with the total EdU counts, expression of CLIMP63 in DRP1 mutant fibroblasts caused a large increase in EdU incorporation in mtDNA present within mitobulbs (Fig. 6B). We then took advantage of the accumulation of EdU foci within mitobulbs to determine whether the reduction in nucleoid size that we observed in CLIMP63-transfected DRP1 mutant cells (Fig. 5C) is due to the rescue of nucleoid segregation from mitobulbs towards the rest of the mitochondrial network. To do that, we chased EdU for 24 hours before fixing the cells. Consistent with our observation that the number of nucleoid-containing mitobulbs was decreased in CLIMP63-expressing cells (Fig. 5G), the number of EdU-positive mitobulbs was decreased in CLIMP63-expressing DRP1 mutant cells, but not the mCherry-expressing cells at 24 hours (Fig. 6B). Importantly, this was not due to the loss of overall EdU staining in mutant cells (Fig. 6C). Overall, our data indicates that modulating ER sheet structure through CLIMP63 expression reactivates both mtDNA replication and nucleoid distribution in DRP1 mutant cells, without altering mitochondrial structure. Thus, proper DRP1-mediated regulation of ER sheet structure is essential to modulate mtDNA replication and nucleoid segregation.

Discussion

mtDNA replication is intimately associated with mitochondrial dynamics, especially mitochondrial fusion which is required for mtDNA replication and integrity (*11, 12*). On the other hand, mitochondrial fission has been associated with nucleoid segregation on the basis of the fact that defects in mitochondrial fission result in nucleoid aggregation within mitobulbs (*13, 15, 16*). With the help of Mitomate Tracker, an automated tool developed in our lab, we have shown that this alters overall nucleoid distribution along mitochondrial networks (*14*). Nevertheless, the mechanism by which DRP1 affects nucleoid distribution remains unclear. Here, we demonstrate that DRP1 regulates mtDNA replication and distribution along mitochondrial network through modulating ER sheet structure.

It is well known that ER tubules regulate mtDNA replication (*19*). However, whether ER sheets also play a role in this process remains unclear. Nevertheless, ER sheets directly interact with mitochondria (Fig. 3) and regulate lipid metabolism in mouse liver cells (*26*), suggesting an important physiological role for this interaction. As we previously showed that, in DRP1 mutants, nucleoids aggregate around the perinuclear region where ER sheets are found (*14*), we further defined how DRP1 impacts this process. Our data demonstrates that DRP1 associates with ER sheets independently of mitochondria and that loss of DRP1 function alters ER sheet structure. Furthermore, DRP1 mutant cells showed increased interaction between ER sheets and mitochondria. Of note, we did not observe distinct changes in ER tubules in our cell models, possibly because ER tubular formation requires the variable domain of DRP1 (*25*) which is still intact in our mutant lines (mutation in the middle domain (G362D))(*28*). Overall, these results indicate that DRP1 regulates ER sheet structure and their interaction with mitochondria.

The altered ER sheets present in DRP1 mutant cells also lead to the accumulation of mtDNA within mitobulbs. Importantly, modulating ER sheets by expressing CLIMP63 recovered nucleoid aggregation and nucleoid number in DRP1 mutants, supporting the idea that ER sheets regulate nucleoid distribution. In addition, our EdU data demonstrate that proper ER sheet structure is necessary to actively regulate mtDNA replication. Altogether, our data show that DRP1-regulated ER sheet structure is essential for both mtDNA replication and distribution, and that this occurs independently of DRP1-dependent changes in mitochondrial structure.

While we demonstrated that ER sheets play an important role in mtDNA replication and distribution, ER tubules are still required. This was shown in a previous study overexpressing CLIMP63 under conditions that caused the complete loss of ER tubules, which significantly reduced mitochondrial DNA replication in cells with wild-type DRP1 (*19*). In contrast, when we expressed CLIMP63 under conditions that do not affect tubular ER structure, it did not impact DRP1 wild-type cells.

Our study also provides novel insights into the defects present in DRP1 mutant patients. Reported human DRP1 mutations are mostly found in the middle and GTPase domains of DRP1, leading to peripheral neuropathy, epilepsy, optic atrophy, and encephalopathy in these patients (*28, 29*). Here, we have used patient fibroblasts with a dominant negative mutation in the middle domain of DRP1 (G362D), leading to refractory epilepsy(*28*). At the cellular level, conditional deletion of DRP1 in

mice affects the movement of mitochondria to the nerve terminal, leading to the loss of dopamine neurons (*30*), while its postnatal deletion in CA1 hippocampal neurons results in functionally impaired mitochondria at the nerve terminals (*31*). Based on our key findings here, we speculate that the altered mtDNA replication and distribution could severely hamper the movement of functional mitochondria towards the synaptic nerve terminal in the patient neurons and thereby impairing neuronal signaling.

Altogether, our results demonstrate the importance of ER sheets in mtDNA maintenance and distribution. However, a number of questions remain. First, we show that DRP1 interacts with ER sheets and regulates its structure, but the underlying mechanism is not fully understood. DRP1 was previously shown to regulate ER tubule formation independently of ER resident dynamics protein and DRP1 receptors (MFF, FIS1) (*25*). Similarly, the expression of some of the major ER dynamics proteins (CLIMP63, RTN4) are not altered in DRP1 mutants, suggesting that DRP1 regulates ER sheets through a direct effect. A second unanswered question relates to the mechanisms through which ER sheets regulate mtDNA replication and distribution. We showed that the interaction between ER sheets and mitochondria was negatively correlated with mtDNA replication and distribution, suggesting the presence of a physical constraint, but this remains to be determined. Overall, our study addresses the novel role of DRP1 on ER sheet structure and its impact on mtDNA replication and distribution.

Materials and Methods

Reagents

Cell culture reagents were obtained from Wisent. Other chemicals were purchased from Sigma-Aldrich, except where indicated.

Cell culture and live cell imaging

Primary human fibroblasts (controls and DRP1 mutants) were generated from skin biopsies, collected as part of an approved research protocol (Research Ethics Board of the Children's Hospital of Eastern Ontario (DRP1 mutants)), and written informed consent from participants was obtained. This study was performed in accordance with the Declaration of Helsinki. Biopsy samples were processed as described and cultured in Dulbecco's modified Eagle's medium (DMEM) containing 10% fetal bovine serum (FBS), supplemented with Penicillin/Streptomycin (100 IU/ml/100µL/mL)(*28*). Immortalized Mouse Embryonic Fibroblasts (MEFs) were cultured in DMEM supplemented with 10% fetal bovine serum. For live cell imaging, cells were seeded onto glass bottom dishes and allowed to adhere to the plate. Then cells were stained for 30 minutes with 250 nM TMRM (Thermo fisher Scientific, T668) and the DNA dye PicoGreen (Thermo Fisher Scientific, P11495) (3 µL/mL). After staining, cells were washed 3 times with pre-warmed 1X phosphate buffered saline (PBS), and normal growth media was added prior to imaging.

Microscopy

Images were acquired with a Leica TSC SP8 confocal microscope fitted with a 63x/1.40 oil objective using the optimal resolution for the wavelength (determined using the Leica software).

siRNA treatment

MEFs were seeded onto 24 well dish and transfected with 15nM of DRP1 siRNA (Thermo Fisher Scientific, Silencer Select, 4390771) and negative siRNA (Thermo Fisher Scientific, Silencer Select, 4390843) using siLenFect lipid reagent (Bio-Rad,1703361). After 48 hrs, cells were treated again with siRNA for another 48 hours. The cells were collected for either western blotting or seeded onto the coverslips for immunofluorescence.

Transient transfection of primary cells

Primary cells were trypsinized and centrifuged at 577 X g for 10 minutes. Cell pellets were suspended in 10µl of the Neon transfection buffer R (ThermoFisher Scientific, MPK1096). Cells were transiently transfected with mCherry (gift from Michael Davidson, Addgene, 54517) and mCherry-tagged CLIMP63 (gift from Gia Voeltz (*32*), Addgene, 136293) using the Neon transfection system (ThermoFisher Scientific, MPK5000) according to the manufacturer's protocol. To minimize effects on ER tubules, minimal concentrations (1µg) of mCherry and mCherry-CLIMP63 plasmids were used.

Immunofluorescence

Cells were seeded onto glass coverslips (Fisherbrand, 1254580) and allowed to adhere overnight. Mitochondria was stained using 50 nM Mitotracker Orange (Thermo fisher scientific, M7510) prior to fixing for certain experiment. Cells were fixed with 4% paraformaldehyde for 15 minutes at room temperature (RT). For antigen retrieval, cells were incubated in sodium citrate buffer (pH 6.0) for 10 minutes at 95°C. Then, cells were permeabilized with 1% BSA / 0.2% Triton X-100 in PBS followed by blocking with 1% BSA / 0.1% Triton X-100 in PBS. The following antibodies were used: CLIMP63 (Rb, Abcam, ab84712, 1:150), CLIMP63 (Mo, ENZO, ENZ-ABS669, 1: 200), DRP1 (Mo, BD Transduction Laboratories, 611112, 1:100), TOM20 (Rb, Abcam, ab186735, 1:250), mtTFAM (Mo, Novusbio, NBP1-71648, 1:150), Calnexin (Mo, Millipore, MABF2067, 1:200), RTN4/NOGOA (Rb, Bio-Rad, AHP1799, 1:200), ATP5a (Mo, Abcam, ab14748, 1:150). Next, cells were incubated with fluorescent tagged secondary antibody (Jackson Immunoresearch, 1:500). To verify the interaction of DRP1 with organelles (ER sheets, mitochondria) or to detect the interaction between organelles (bulb-like mitochondria and ER sheets), line scan analysis was performed using the *RGB profiler* in Image J. ER and mitochondrial structures were manually quantified by binning them into the indicated categories.

Proximity Ligation Assay (PLA)

Cells were grown on glass coverslips and fixed with 4% paraformaldehyde. Following antigen retrieval, cells were permeabilized with 1% BSA/0.2% Triton X-100 in PBS for 15 minutes at RT. The ER was marked with an antibody recognizing CLIMP63 or calnexin and mitochondria was marked with an antibody recognizing TOM20. The PLA assays were performed using Duolink In Situ green kit Mouse/ Rabbit (Sigma Aldrich) following the manufacturer's protocol. The primary antibodies were then labelled using fluorescent-tagged secondary antibodies. Total and mitobulb associated PLA foci were manually counted at the site of CLIMP63-TOM20 signal while overall calnexin-TOM20 foci were quantified using the *analyze particles* function in ImageJ.

Transmission Electron Microscopy (TEM)

Primary fibroblasts were seeded on Nunc Lab-Tek chamber slides (Thermo Fisher Scientific, 177437) and allowed to adhere overnight. Cells were washed with 0.1M sodium cacodylate buffer (pH 7.3) and fixed with 2.5% glutaraldehyde in 0.1M sodium cacodylate buffer (pH 7.3), overnight at 4°C. Fixed cells were further processed in McGill's facility for electron microscopy research (FEMR). Images were acquired using a EMS208S electron microscope (Philips) by an independent trained operator in University of Quebec in Trois-Rivières' TEM facility. ER sheet-mitochondrial contact sites in the perinuclear region was manual quantified, considering only contact sites ≤ 30 nm based on a previous study (*33*). To measure changes in ER structure we considered rough ER as 'sheets' and smooth ER as 'tubules'. We manually measured ER surface area and luminal width for 10 randomly chosen ER sheets/tubules in each of the four quadrants per image of the cell.

Western Blot

Cell were lysed in 10 mM Tris-HCl, pH 7.4, 1mM EDTA, 150 mM NaCl, 1% Triton X-100, 50 mM sodium fluoride, complemented with a protease inhibitor cocktail (Sigma-Aldrich), centrifuged at 15890 X g for 5 minutes and protein supernatants collected. Protein concentrations were estimated calorimetrically by DC protein assay kit (BioRad). For SDS-PAGE, 20 µg (siRNA treatment in MEFs)/25 µg (Mitochondrial and ER proteins in human fibroblasts) of proteins were mixed with 1X Lammeli buffer containing β-mercaptoethanol, then subjected to SDS-PAGE, transferred to nitrocellulose membranes and blotted with the indicated antibodies (DRP1 (BD Transduction Laboratories, 611112, 1:1000), CLIMP63 (Mo, ENZO, ENZ-ABS669, 1: 500), TOM20 (Rb, Abcam, ab186735, 1:1000), Calnexin (Mo, Millipore, MABF2067, 1:1000), RTN4/NOGOA (Rb, Bio-Rad, AHP1799, 1:1000), ATP5a (Mo, Abcam, ab14748, 1:1000), HRP-tagged Actin (1:10,000). Membranes were then incubated with a 1:5000 dilution of horseradish peroxidase-conjugated secondary antibodies (Jackson Immunoresearch) and visualized by enhanced chemiluminescence (Thermo Fisher scientific) using a Bio-Rad imaging system.

EdU Labeling

Primary fibroblasts (Control and DRP1 mutants) were incubated with 60µM EdU for 2 hours at 37°C. For the chase experiments, the EdU containing media was replaced with fresh media and incubated further for 24 hours. Cells were then fixed with 4% paraformaldehyde for 15 minutes at RT, permeabilized and EdU detected using Click-iT EdU imaging kit (Thermo Fisher Scientific, C10337). Cells were then immunolabelled for TOM20 (Abcam, ab186735, 1:250). EdU foci in mitobulbs and total EdU foci were manually counted.

Data analysis and statistics

All graphs and statistical analysis were done using R. Immunofluorescence data were quantified and images representative of at least three independent experiments shown (exact n are in the quantification figures). Data are represented as average ± SD as specified in figure legends. Statistical significance was determined using Student's t test (between 2 groups) or one-way ANOVA with a tukey post hoc test (multiple comparisons).

Acknowledgements

This work was supported by grants from the Natural Sciences and Engineering Research Council of Canada and the Fondation de l'UQTR to MG. HSI was supported by a Queen Elizabeth II Diamond Jubilee Scholarship and a FRQ-NT scholarship.

Author contribution

HSI performed the cell biology experiments. HSI and MG designed the experiments. HSI, JDG, SB and MG analysed the data. MAL provided the clinical samples. HSI and MG wrote the paper. All authors reviewed and discussed the manuscript.

References

1. J. B. Spinelli, M. C. Haigis, The multifaceted contributions of mitochondria to cellular metabolism. *Nature Cell Biology* **20**, 745-754 (2018).
2. F. J. Bock, S. W. G. Tait, Mitochondria as multifaceted regulators of cell death. *Nature Reviews Molecular Cell Biology* **21**, 85-100 (2019).
3. C. Giorgi, S. Marchi, P. Pinton, The machineries, regulation and cellular functions of mitochondrial calcium. *Nature Reviews Molecular Cell Biology* **19**, 713-730 (2018).
4. Gerald S. Shadel, Tamas L. Horvath, Mitochondrial ROS Signaling in Organismal Homeostasis. *Cell* **163**, 560-569 (2015).
5. P. Lisowski, P. Kannan, B. Mlody, A. Prigione, Mitochondria and the dynamic control of stem cell homeostasis. *EMBO reports* **19**, (2018).
6. V. Tiku, M.-W. Tan, I. Dikic, Mitochondrial Functions in Infection and Immunity. *Trends in Cell Biology* **30**, 263-275 (2020).
7. H. Otera *et al.*, Mff is an essential factor for mitochondrial recruitment of Drp1 during mitochondrial fission in mammalian cells. *Journal of Cell Biology* **191**, 1141-1158 (2010).
8. O. C. Losón, Z. Song, H. Chen, D. C. Chan, D. D. Newmeyer, Fis1, Mff, MiD49, and MiD51 mediate Drp1 recruitment in mitochondrial fission. *Molecular Biology of the Cell* **24**, 659-667 (2013).
9. H. Chen *et al.*, Mitofusins Mfn1 and Mfn2 coordinately regulate mitochondrial fusion and are essential for embryonic development. *Journal of Cell Biology* **160**, 189-200 (2003).
10. S. Cipolat, O. M. de Brito, B. Dal Zilio, L. Scorrano, OPA1 requires mitofusin 1 to promote mitochondrial fusion. *Proceedings of the National Academy of Sciences* **101**, 15927-15932 (2004).
11. E. Silva Ramos *et al.*, Mitochondrial fusion is required for regulation of mitochondrial DNA replication. *PLOS Genetics* **15**, (2019).
12. H. Chen *et al.*, Mitochondrial Fusion Is Required for mtDNA Stability in Skeletal Muscle and Tolerance of mtDNA Mutations. *Cell* **141**, 280-289 (2010).
13. R. Ban-Ishihara, T. Ishihara, N. Sasaki, K. Mihara, N. Ishihara, Dynamics of nucleoid structure regulated by mitochondrial fission contributes to cristae reformation and release of cytochrome c. *Proceedings of the National Academy of Sciences* **110**, 11863-11868 (2013).
14. H. S. Ilamathi *et al.*, A new automated tool to quantify nucleoid distribution within mitochondrial networks. *Scientific reports* **11**, 22755 (2021).
15. T. Ishihara *et al.*, Dynamics of Mitochondrial DNA Nucleoids Regulated by Mitochondrial Fission Is Essential for Maintenance of Homogeneously Active Mitochondria during Neonatal Heart Development. *Molecular and Cellular Biology* **35**, 211-223 (2015).
16. N. Ishihara, T. Ishihara, A. Ota, Mitochondrial nucleoid morphology and respiratory function are altered in Drp1-deficient HeLa cells. *The Journal of Biochemistry* **167**, 287-294 (2020).
17. R. G. Abrisch, S. C. Gumbin, B. T. Wisniewski, L. L. Lackner, G. K. Voeltz, Fission and fusion machineries converge at ER contact sites to regulate mitochondrial morphology. *Journal of Cell Biology* **219**, (2020).
18. J. R. Friedman *et al.*, ER Tubules Mark Sites of Mitochondrial Division. *Science* **334**, 358-362 (2011).
19. S. C. Lewis, L. F. Uchiyama, J. Nunnari, ER-mitochondria contacts couple mtDNA synthesis with mitochondrial division in human cells. *Science* **353**, (2016).
20. J. R. Friedman, G. K. Voeltz, The ER in 3D: a multifunctional dynamic membrane network. *Trends in Cell Biology* **21**, 709-717 (2011).
21. D. S. Schwarz, M. D. Blower, The endoplasmic reticulum: structure, function and response to cellular signaling. *Cellular and Molecular Life Sciences* **73**, 79-94 (2015).

22. Y. Shibata *et al.*, Mechanisms Determining the Morphology of the Peripheral ER. *Cell* **143**, 774-788 (2010).
23. H. Zhang, J. Hu, Shaping the Endoplasmic Reticulum into a Social Network. *Trends in Cell Biology* **26**, 934-943 (2016).
24. W.-K. Ji *et al.*, Receptor-mediated Drp1 oligomerization on endoplasmic reticulum. *Journal of Cell Biology* **216**, 4123-4139 (2017).
25. Y. Adachi *et al.*, Drp1 Tubulates the ER in a GTPase-Independent Manner. *Molecular Cell* **80**, 621-632.e626 (2020).
26. I. Anastasia *et al.*, Mitochondria-rough-ER contacts in the liver regulate systemic lipid homeostasis. *Cell Reports* **34**, (2021).
27. E. Smirnova, L. Griparic, D.-L. Shurland, A. M. van der Bliek, T. D. Pollard, Dynamin-related Protein Drp1 Is Required for Mitochondrial Division in Mammalian Cells. *Molecular Biology of the Cell* **12**, 2245-2256 (2001).
28. J. R. Vanstone *et al.*, DNM1L-related mitochondrial fission defect presenting as refractory epilepsy. *European Journal of Human Genetics* **24**, 1084-1088 (2015).
29. R. Banerjee, A. Mukherjee, S. Nagotu, Mitochondrial dynamics and its impact on human health and diseases: inside the DRP1 blackbox. *Journal of Molecular Medicine*, (2021).
30. A. Berthet *et al.*, Loss of Mitochondrial Fission Depletes Axonal Mitochondria in Midbrain Dopamine Neurons. *Journal of Neuroscience* **34**, 14304-14317 (2014).
31. L. Y. Shields *et al.*, Dynamin-related protein 1 is required for normal mitochondrial bioenergetic and synaptic function in CA1 hippocampal neurons. *Cell Death & Disease* **6**, e1725-e1725 (2015).
32. Y. Shibata *et al.*, The reticulon and DP1/Yop1p proteins form immobile oligomers in the tubular endoplasmic reticulum. *The Journal of biological chemistry* **283**, 18892-18904 (2008).
33. G. r. Csordás *et al.*, Structural and functional features and significance of the physical linkage between ER and mitochondria. *Journal of Cell Biology* **174**, 915-921 (2006).

Figure Legends

Figure 1. DRP1 regulates ER sheet structure. (A) DRP1 associates with ER sheets. Representative image of control human fibroblasts showing DRP1 (Green), mitochondria (Mitotracker orange, Blue) and ER sheets (CLIMP63, Red). Left panel, Colocalization of DRP1 with mitochondria (arrows) and ER sheets (arrowheads). Line scan analysis confirmed the colocalization (image, middle panel; line scan, right panel). **The full cell is shown in Sup. Fig. 1A** (B-D) ER sheet structure is affected in DRP1 mutant fibroblasts. (B) Representative images of CLIMP63 staining in control and DRP1 mutant fibroblasts. (C) Quantification of ER sheet structure as Structured (Blue) or Altered (red; presence of punctate structures and thick ER sheet patches). Each point represents one independent experiment, with at least 20 cells quantified per experiment. Bars show the average ± SD. * $p<0.05$, ** $p<0.01$ One-way ANOVA using the data for Structured ER. (D) Quantification of ER sheet surface area relative to the total cell area (determined by Differential interference contrast (DIC)). Each data point represents one cell. Bars represent the average of 35 cells in 3 independent experiments ± SD *** $p<0.001$ two-sided t-test. (E-G) ER sheet structure is affected in MEFs knocked down for DRP1. (F) Quantification of ER sheet structure as Structured (Blue) or Altered (red; presence of punctate structures and thick ER sheet patches). Each point represents one independent experiment, with at least 20 cells quantified per experiment. Bars show the average ± SD. * $p<0.05$, Two-sided t-test using the data for Structured ER. (D) Quantification of ER sheet surface area relative to the total cell area (determined by DIC). Each data point represents one cell. Bars represent the average of 54 cells in 3 independent experiments ± SD. ** $p<0.01$ two-sided t-test. Scale bars 10 µm, 2 µm for the zoomed images in (A).

Figure 2. EM analysis of ER sheets and tubules in DRP1 mutant cells. (A) Representative EM images. Asterisks denote ER sheets (Top) or ER tubules (Bottom). Scale bar 500 nm. (B-C) Quantification of the average ER sheet area (B) and luminal width (C). Each data point represents one cell. Bars represent the average of 10 cells ± SD ** $p<0.01$ two-sided t-test. (D-E) Quantification of the average ER tubule area (D) and luminal width (E). Each data point represents one cell. Bars represent the average of 10 cells ± SD. ns, not significant. two-sided t-test.

Figure 3. DRP1 regulates the interaction between ER sheets and mitochondria. (A) Representative images of control and DRP1 mutant fibroblasts showing the PLA for CLIMP63 and TOM20 (White), along with CLIMP63 (red), TOM20 (Green) and nuclei (Hoechst, Blue). Scale bar 10 µm, 2 µm for the zoomed images. (B) Quantification of CLIMP63-TOM20 PLA. Each data point represents one cell. Bars represent the average of 50 control and 48 mutant cells in 3 independent experiments ± SD *** $p<0.001$ two-sided t-test (C) Quantification of Calnexin-TOM20 PLA. Each data point represents one cell. Bars represent the average of 40 cells per genotype in 3 independent experiments ± SD ** $p<0.01$ two-sided t-test (D) Representative TEM images of control and DRP1 mutant fibroblasts. Scale bar 500 nm (E) Quantification of the number of ERMCS per mitochondrial length in the TEM images. Each data point represents one

mitochondrion. Bars represent the average of 103 control and 97 mutant mitochondria ± SD ** $p<0.01$ two-sided t-test (F) Quantification of ERMCs length (µm) per mitochondria in the TEM images. Each data point represents one mitochondrion. Bars represent the average of 103 control and 97 mutant mitochondria ± SD *** $p<0.001$ two-sided t-test.

Figure 4. Modified ER sheets are associated with mitobulbs. (A) Representative live cell images showing the mitochondrial marker, TMRM and picogreen-stained DNA in control and DRP1 mutant human fibroblasts. The zoomed images show the enlarged nucleoids present in mitobulbs (arrowheads). (B-D) Colocalisation between ER sheets and mitobulbs. Colocalisation was measured in cells immunolabelled for CLIMP63 (ER sheets) and ATP5a (mitochondria). (B) representative images. (C) Line scan analysis along the line shown in the zoomed images in (B). (D) Quantification of the percent of mitobulbs that are associated with CLIMP63-positive ER sheets in two independent DRP1 mutant lines (P1 and P2). Each data point represents one cell. Bars represent the average of 45 control and 45 mutant mitochondria ± SD. (E-F) Interaction between ER sheets and mitobulbs as measured by PLA for TOM20 and CLIMP63 or Calnexin. (E) Representative image of TOM20-CLIMP63 PLA. Arrowheads denote PLA foci (White) on mitobulbs (TOM20, Green) at sites where they contact ER sheets (CLIMP63, Red). (F) Quantification of mitobulbs associated with PLA foci for TOM20-CLIMP63 and TOM20-Calnexin. Each data point represents one cell. Bars represent the average of 48 (CLIMP63 PLA) and 40 cells (Calnexin PLA) in 3 independent experiments ± SD. Scale bars 10 µm, 2 µm for the zoomed images in (A), (B) and (E).

Figure 5. CLIMP63 expression rescues nucleoid distribution in DRP1 mutant fibroblasts. (A-B) Quantification of PLA foci (CLIMP63-TOM20) in mCherry and mCherrry-CLIMP63 expressing control and DRP1 mutant cells. Total PLA foci (A) and mitobulbs associated with PLA foci (B) were quantified. Each point represents one cell, with at least 43 cells quantified per condition in 3 independent experiments. Bars show the average ± SD. One-way ANOVA. ** $p<0.01$, *** $p<0.001$, ns not significant. One-way ANOVA (C) Quantification of nucleoid area in mCherry and mCherry-CLIMP63 expressing control and DRP1 mutants from images in Figure S5. Each point represents one cell, with at least 32 cells quantified per condition in 3 independent experiments. Bars show the average ± SD. One-way ANOVA. *** $p<0.001$, ns not significant. One-way ANOVA. (D-E) Mitobulbs are mtDNA clusters. (D) Representative images of mCherry-expressing DRP1 mutants labeled for EdU (green) and TOM20 (mitochondria). Arrowheads indicate EdU-positive mtDNA in mitobulbs. Scale bar 10µm (E). Quantification of number of EdU foci/mitobulb. Each point represents an individual cell, with 45 cells quantified in 3 independent experiments. Bars show the average ± SD. (F-H) Rescue of nucleoid numbers in CLIMP63-expressing cells. Quantification of total nucleoids (TFAM-positive, F), mitobulbs containing nucleoids (TFAM-positive, G) and mitochondrial bulb-like structures (independently of the presence of nucleoids, H) in mCherry and mCherrry-CLIMP63 expressing control and DRP1 mutant cells. Each point represents one cell, with 40 mCherry (mch) and 47 mCherry-CLIMP63

cells quantified in 3 independent experiments. Bars show the average ± SD. One way ANOVA (F), two-sided t-test (G, H). * $p<0.05$, *** $p<0.001$, ns, not significant.

Figure 6. CLIMP63 expression rescues mtDNA replication and distribution in DRP1 mutant fibroblasts. (A) Quantification of EdU foci in control and DRP1 mutants expressing mCherry or mCherry-CLIMP63 in cells labelled with EdU for 4 hours. Each point represents one cell, with at least 43 cells quantified in 3 independent experiments. Bars show the average ± SD. One way ANOVA. * $p<0.05$, *** $p<0.001$, ns not significant. (B) Quantification of EdU-positive mitobulbs in EdU-labelled DRP1 mutants expressing mCherry or mCherry-CLIMP63. Cells were pulsed with EdU as in (A) then the EdU was chased for 24 hours where indicated. Each point represents one cell, with at least 44 cells quantified in 3 independent experiments. Bars show the average ± SD. One way ANOVA. *** $p<0.001$. (C) EdU foci ratio (chase/no chase) from the experiments in (A-B). Each point represents one independent experiment (n=3). Bars show the average ± SD. Two-sided t-test. ns not significant.

Supplementary Figure 1. Structure of ER tubules in DRP1 mutant cells. (A) Representative image of control human fibroblasts showing DRP1 (Green), mitochondria (Mitotracker orange, Blue) and ER sheets (CLIMP63, Red). The box shows the area that is enlarged in Figure 1A. (B) WB showing DRP1 expression in WT MEFs transfected with a control siRNA (siCtrl) or a siRNA against DRP1 (siDRP1). (C) WB showing ER (CLIMP63, RTN4, calnexin) and mitochondrial proteins (TOM20, ATP5a) in control and DRP1 mutant human fibroblasts. (D) Representative images showing the RTN4 in MEFs transfected with control and DRP1 siRNAs. Scale bar 10 µm, 2 µm for the zoomed images. (E) Representative images showing RTN4 in control and DRP1 mutant human fibroblasts. Scale bar 10 µm, 2 µm for the zoomed images.

Supplementary Figure 2. Calnexin-TOM20 PLA. (A) Representative image of PLA (IgG and TOM20; white) for the antibody control (IgG), along with IgG (red), TOM20 (green) and nuclei (Hoechst, Blue) in control fibroblasts. (B) Representative images of control and DRP1 mutant fibroblasts showing the PLA for Calnexin and TOM20 (white), along with Calnexin (red), TOM20 (Green) and nuclei (Hoechst, Blue). (C) Zoomed in image of DRP1 mutant. Arrowheads denote PLA foci on mitobulbs. Scale bar 10 µm, 2 µm for the zoomed images.

Supplementary Figure 3. ER tubules are not affected by CLIMP63 expression. (A) Representative images of Control cells expressing mCherry and mCherry-CLIMP63 (Magenta) and immunolabelled for RTN4 (green). Scale bar 10 µm, 2 µm for the zoomed images. (B) Quantification of mitochondrial phenotypes (short (green), intermediate (red), elongated (blue)) in mCherry and mCherry-CLIMP63 expressing control and DRP1 mutant fibroblasts. Each point

represents an independent experiment. Bars show the average ± SD. Two-way ANOVA. *** $p<0.001$, ns not significant.

Supplementary Figure 4. CLIMP63 expression alters ER sheet structure in control and DRP1 mutants. Representative images of control and DRP1 mutant fibroblasts expressing mCherry or mCherry-CLIMP63 (Magenta) and immunolabelled for CLIMP63 (ER sheets, green). Scale bar 10 µm.

Supplementary Figure 5. CLIMP63 expression rescues nucleoid aggregation in DRP1 mutants. Representative images of control and DRP1 mutant fibroblasts expressing mCherry or mCherry-CLIMP63 (blue) immunolabeled for TFAM (nucleoids, Green) and TOM20 (mitochondria, Red). Scale bar 10 µm.

Figure 1

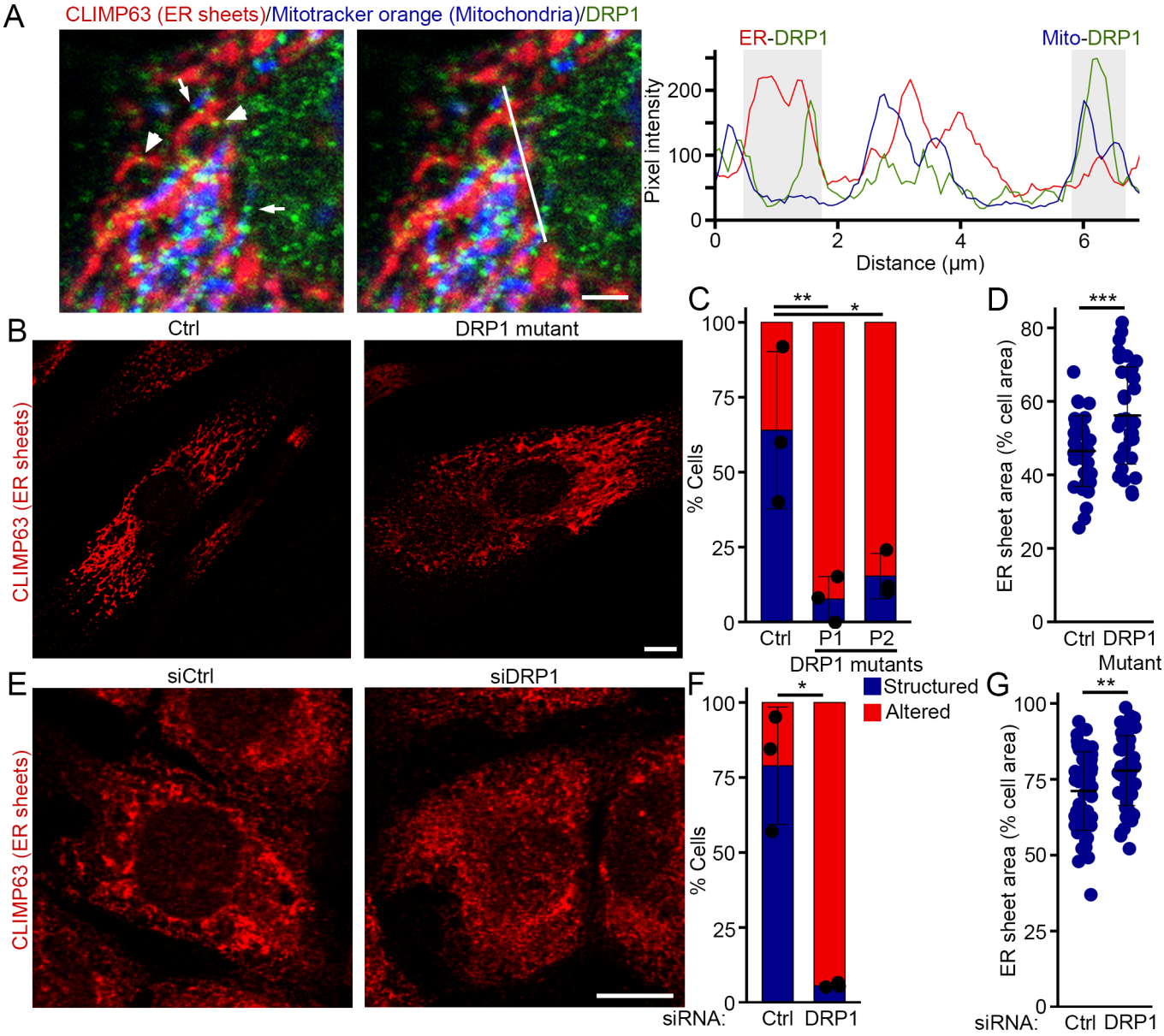
A
CLIMP63 (ER sheets)/Mitotracker orange (Mitochondria)/DRP1
ER-DRP1
Mito-DRP1
Pixel intensity
Distance (µm)
B
Ctrl
DRP1 mutant
CLIMP63 (ER sheets)
C
% Cells
Ctrl
P1
P2
DRP1 mutants
D
ER sheet area (% cell area)
Ctrl
DRP1 Mutant
E
siCtrl
siDRP1
CLIMP63 (ER sheets)
F
Structured
Altered
% Cells
siRNA:
Ctrl
DRP1
G
ER sheet area (% cell area)
siRNA:
Ctrl
DRP1

Figure 2

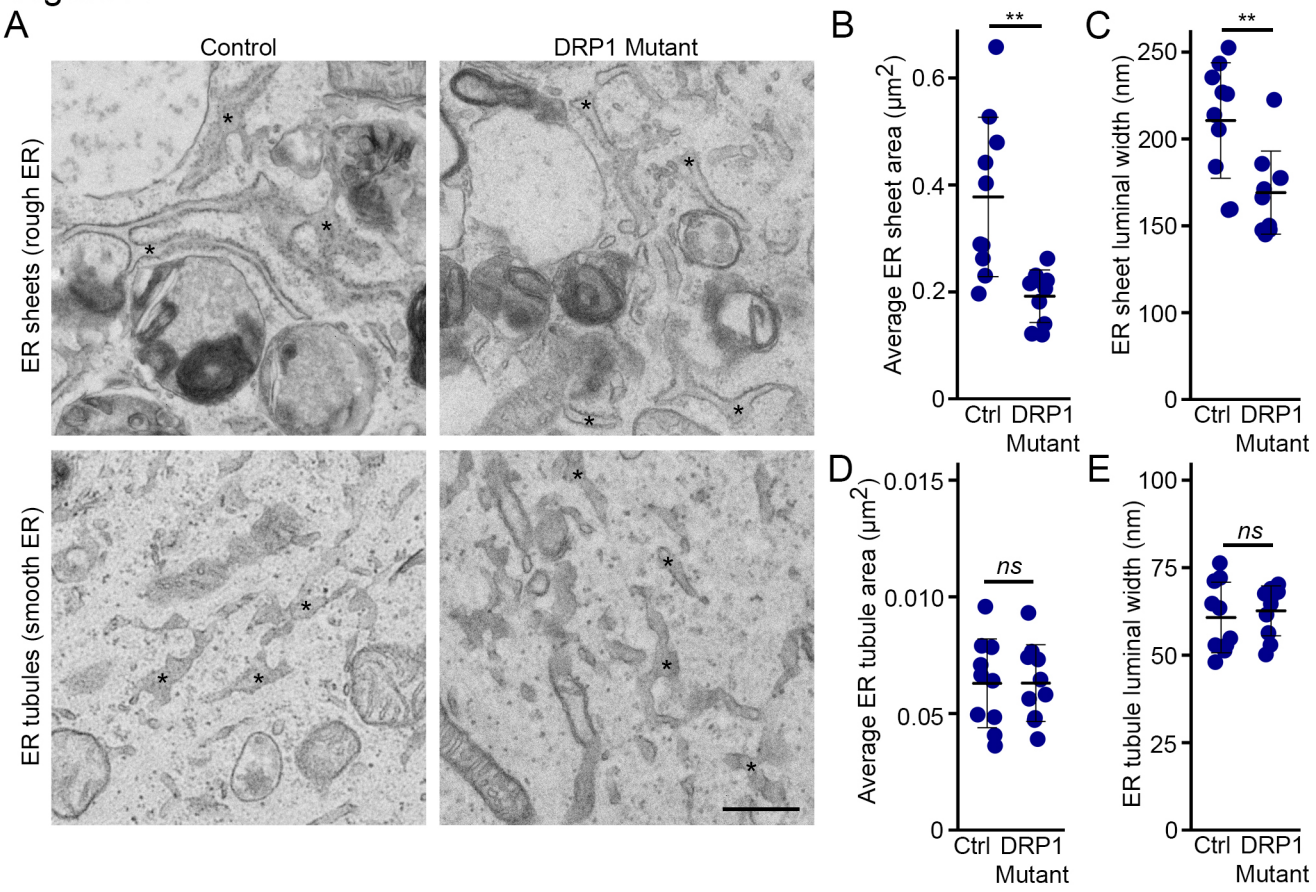
A
Control
DRP1 Mutant
ER sheets (rough ER)
ER tubules (smooth ER)
B
Average ER sheet area (μm2)
0
0.2
0.4
0.6
**
Ctrl
DRP1 Mutant
C
ER sheet luminal width (nm)
0
100
150
200
250
**
Ctrl
DRP1 Mutant
D
Average ER tubule area (μm2)
0
0.05
0.010
0.015
ns
Ctrl
DRP1 Mutant
E
ER tubule luminal width (nm)
0
25
50
75
100
ns
Ctrl
DRP1 Mutant

Figure 3

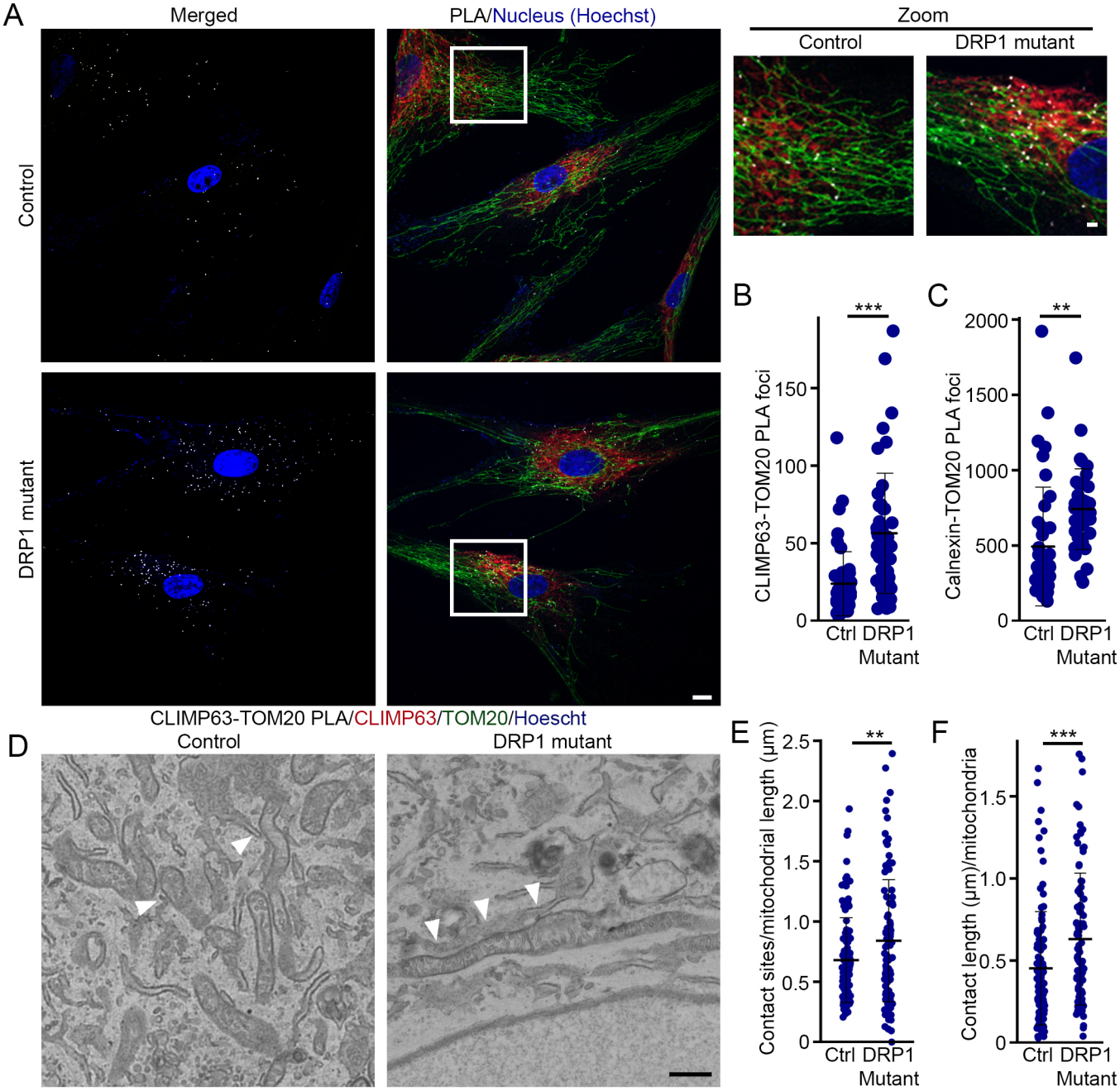
A
Merged
PLA/Nucleus (Hoechst)
Zoom
Control
DRP1 mutant
Control
DRP1 mutant
B
***
CLIMP63-TOM20 PLA foci
150
100
50
0
Ctrl
DRP1 Mutant
C
**
Calnexin-TOM20 PLA foci
2000
1500
1000
500
0
Ctrl
DRP1 Mutant
CLIMP63-TOM20 PLA/CLIMP63/TOM20/Hoescht
D
Control
DRP1 mutant
E
**
Contact sites/mitochodrial length (µm)
2.5
2.0
1.5
1.0
0.5
0
Ctrl
DRP1 Mutant
F
***
Contact length (µm)/mitochondria
1.5
1.0
0.5
0
Ctrl
DRP1 Mutant

Figure 4

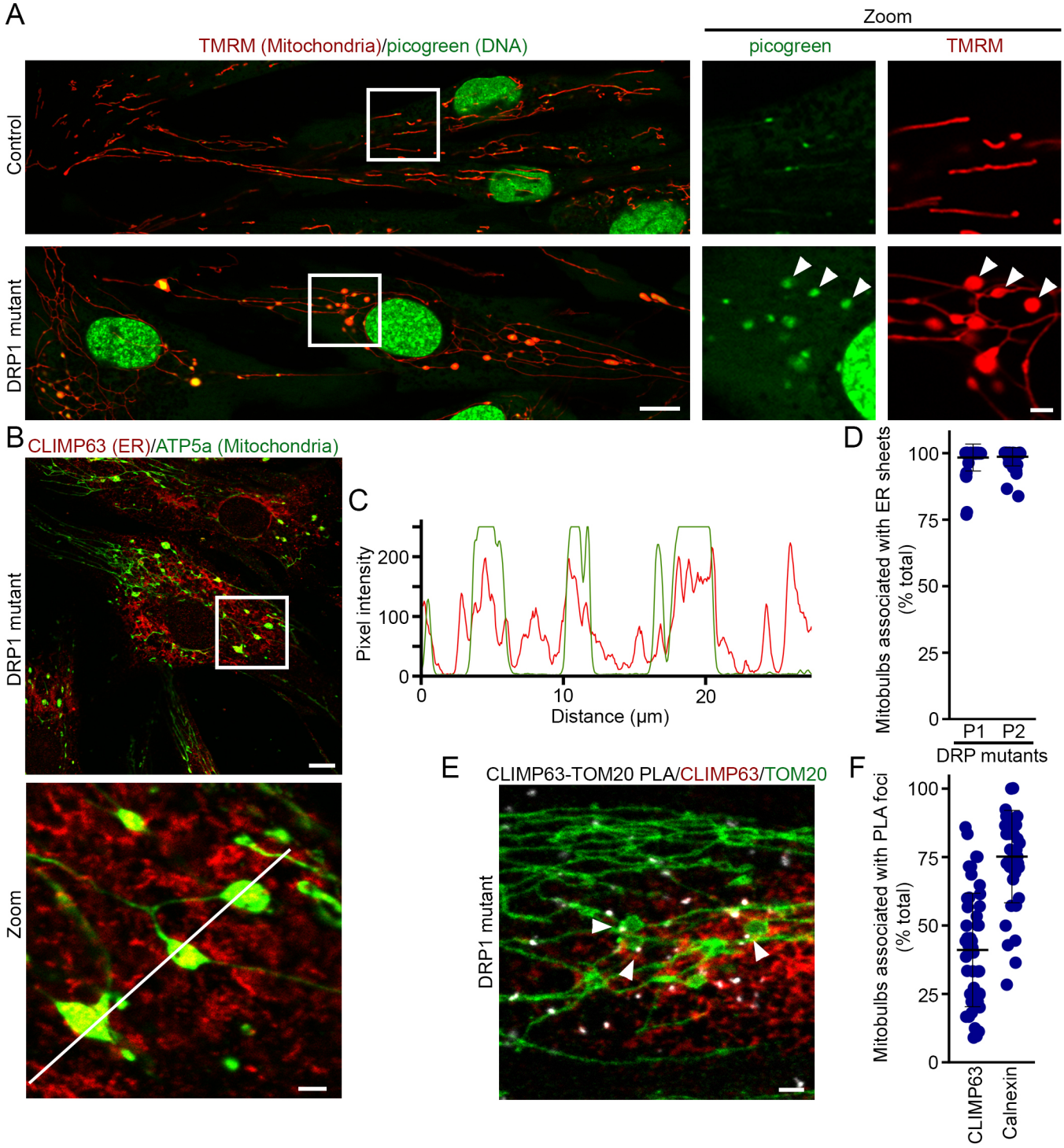
A
Zoom
TMRM (Mitochondria)/picogreen (DNA)
picogreen
TMRM
Control
DRP1 mutant
B
CLIMP63 (ER)/ATP5a (Mitochondria)
DRP1 mutant
Zoom
C
Pixel intensity
200
100
0
0
10
20
Distance (μm)
D
Mitobulbs associated with ER sheets (% total)
100
75
50
25
0
P1
P2
DRP mutants
E
CLIMP63-TOM20 PLA/CLIMP63/TOM20
DRP1 mutant
F
Mitobulbs associated with PLA foci (% total)
100
75
50
25
0
CLIMP63
Calnexin

Figure 5

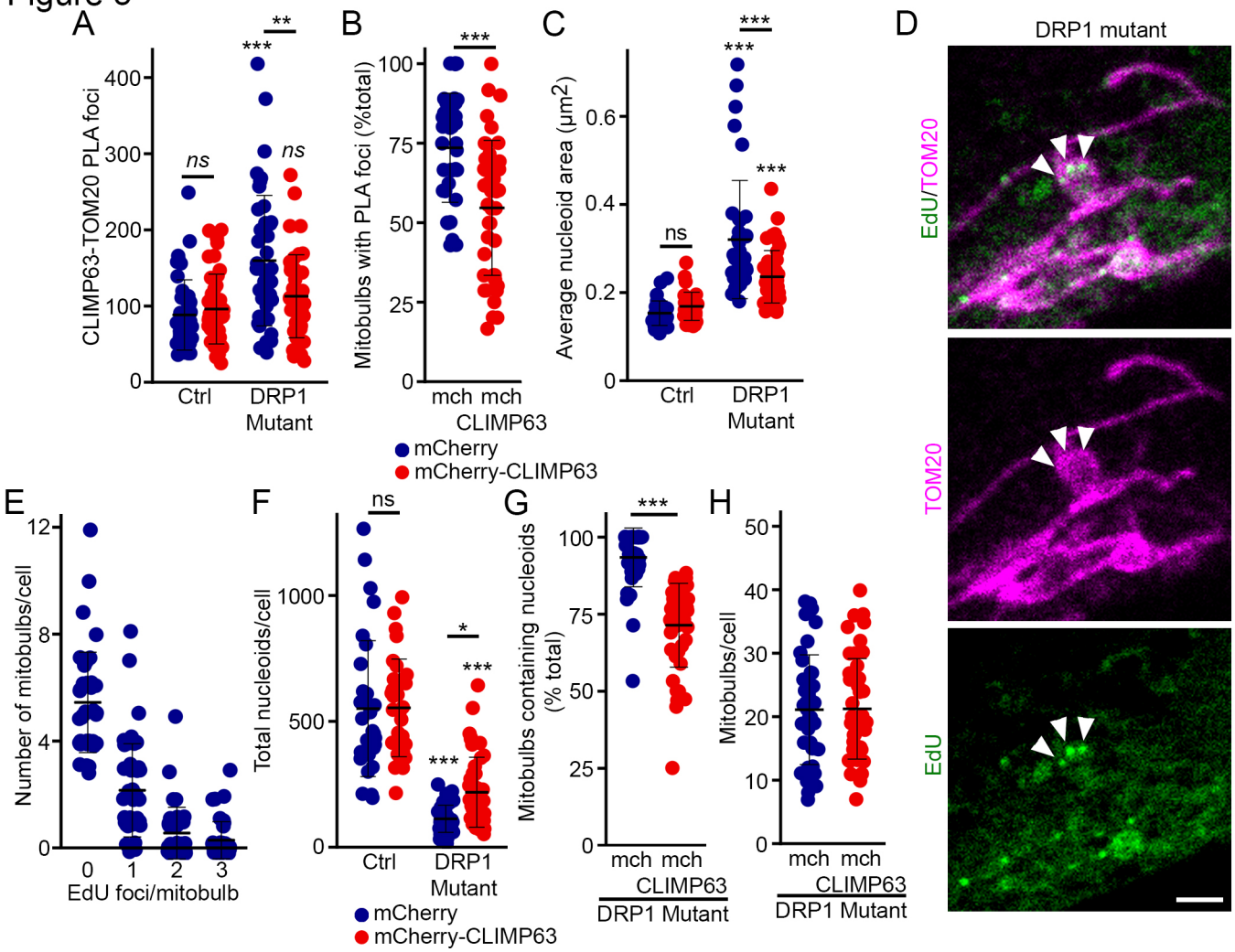
A
CLIMP63-TOM20 PLA foci
400
300
200
100
0
ns
***
ns
**
Ctrl
DRP1 Mutant
B
Mitobulbs with PLA foci (%total)
100
75
50
25
0
***
mch mch
CLIMP63
C
Average nucleoid area (μm2)
0.6
0.4
0.2
0
ns
***
***
***
Ctrl
DRP1 Mutant
mCherry
mCherry-CLIMP63
D
DRP1 mutant
EdU/TOM20
TOM20
EdU
E
Number of mitobulbs/cell
12
8
4
0
0 1 2 3
EdU foci/mitobulb
F
Total nucleoids/cell
1000
500
0
ns
*
***
***
Ctrl
DRP1 Mutant
mCherry
mCherry-CLIMP63
G
Mitobulbs containing nucleoids (% total)
100
75
50
25
0
***
mch mch
CLIMP63
DRP1 Mutant
H
Mitobulbs/cell
50
40
30
20
10
0
mch mch
CLIMP63
DRP1 Mutant

Figure 6

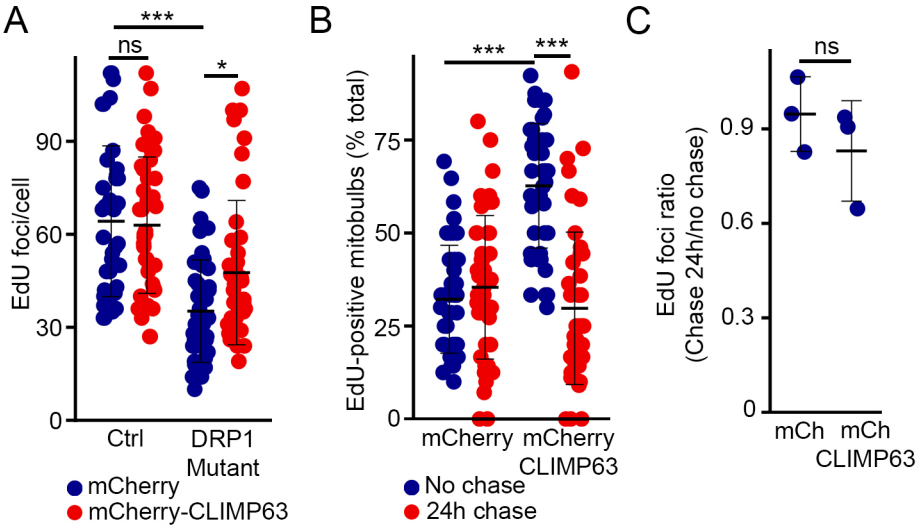
A
***
ns
*
EdU foci/cell
90
60
30
0
Ctrl
DRP1 Mutant
mCherry
mCherry-CLIMP63
B
***
***
EdU-positive mitobulbs (% total)
75
50
25
0
mCherry
mCherry CLIMP63
No chase
24h chase
C
ns
EdU foci ratio (Chase 24h/no chase)
0.9
0.6
0.3
0
mCh
mCh CLIMP63

Supplementary Figure 1

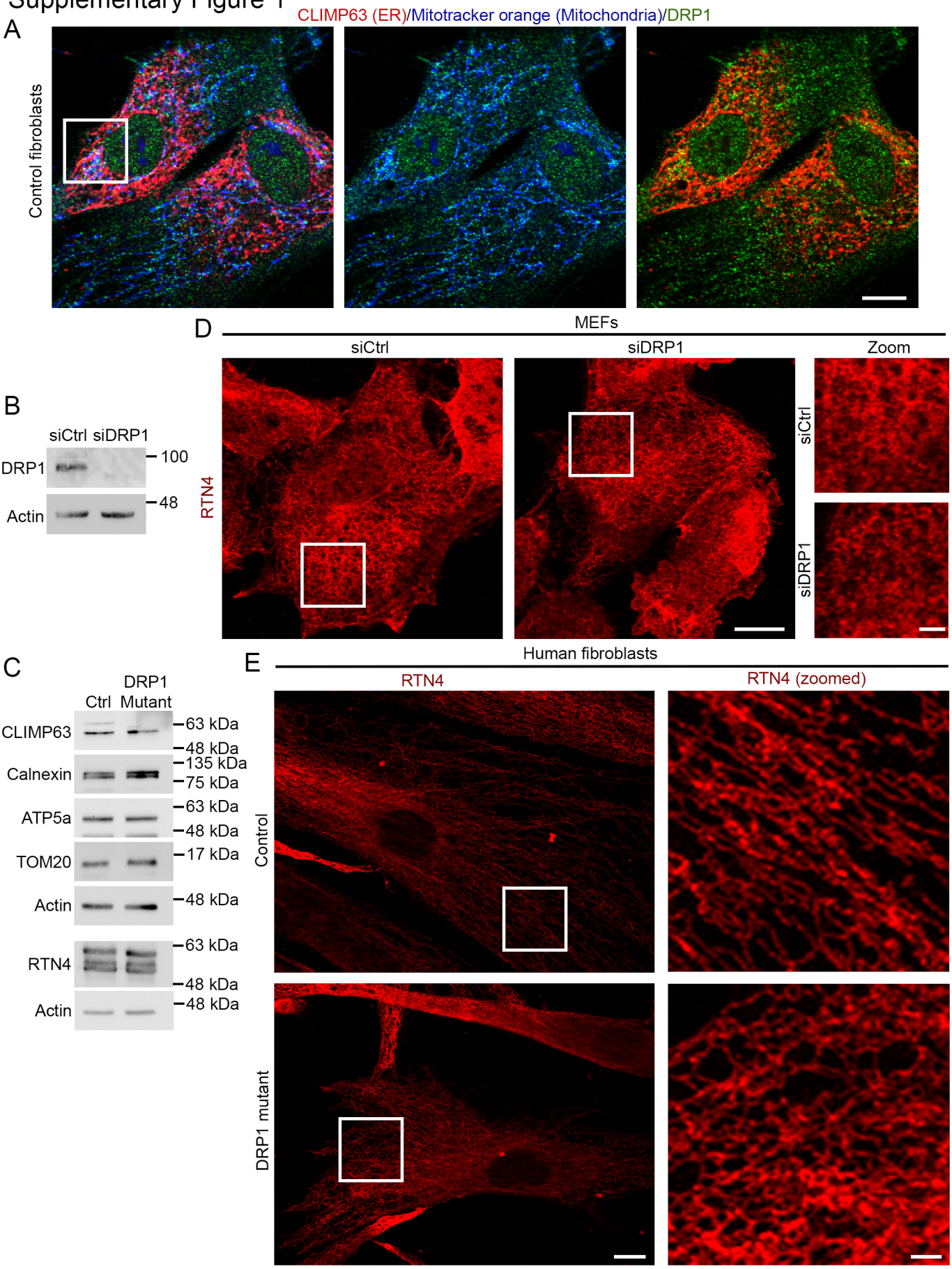

Supplementary Figure 2

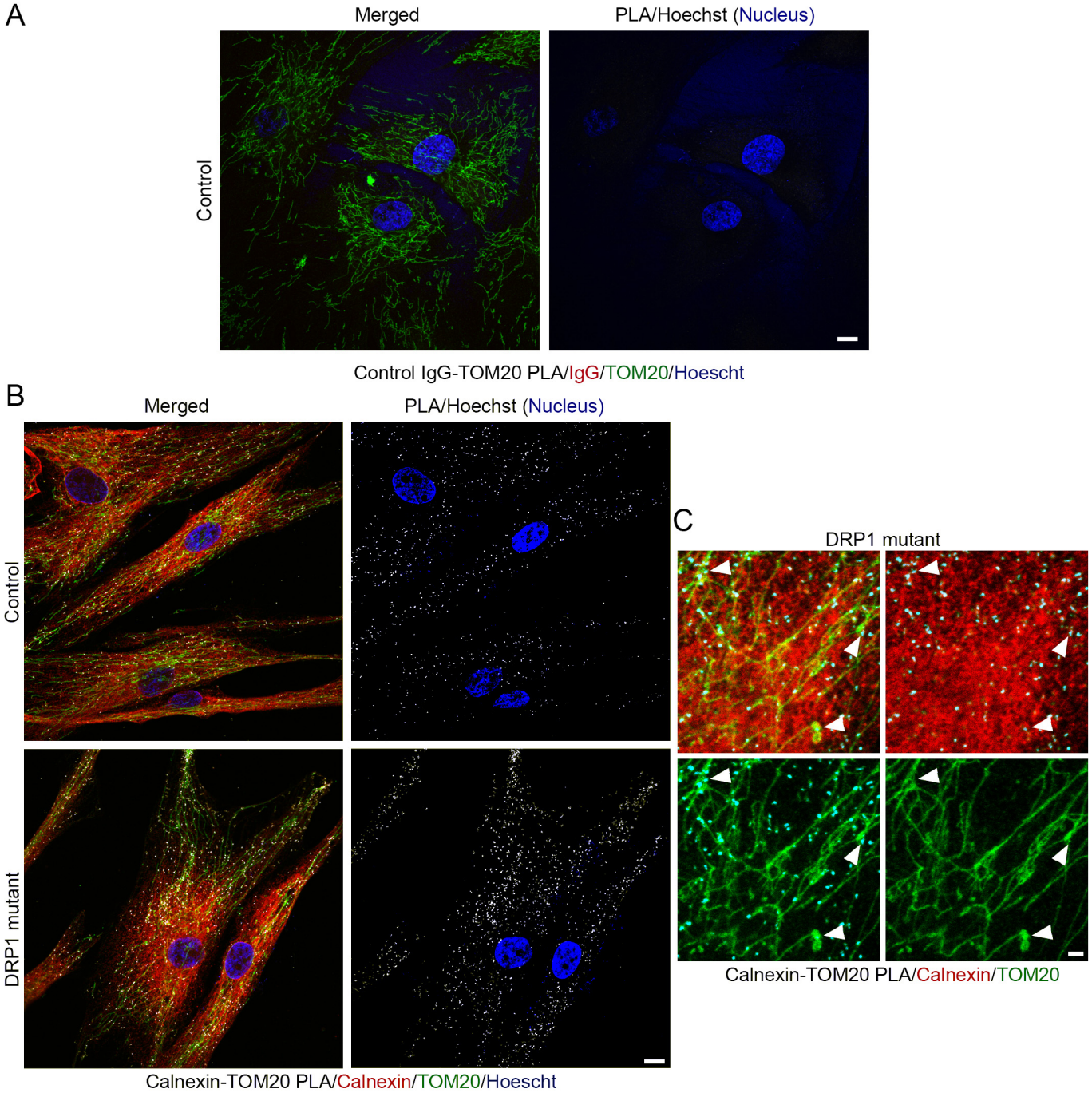

Sup. Figure 3

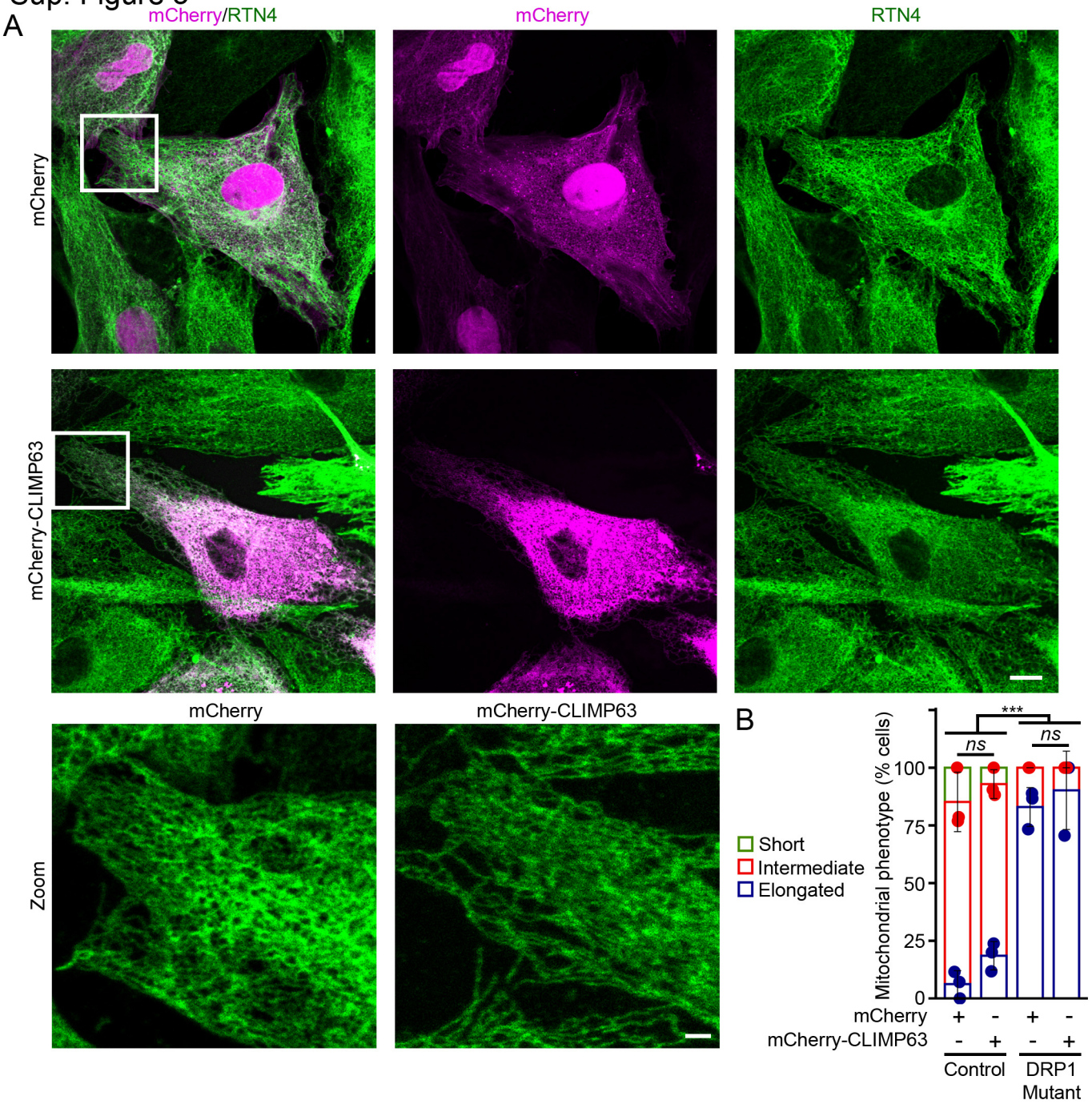
A
mCherry/RTN4
mCherry
RTN4
mCherry
mCherry-CLIMP63
mCherry
mCherry-CLIMP63
Zoom
B
Short
Intermediate
Elongated
Mitochondrial phenotype (% cells)
100
75
50
25
0
***
ns
ns
mCherry
mCherry-CLIMP63
Control
DRP1 Mutant

Sup. Figure 4

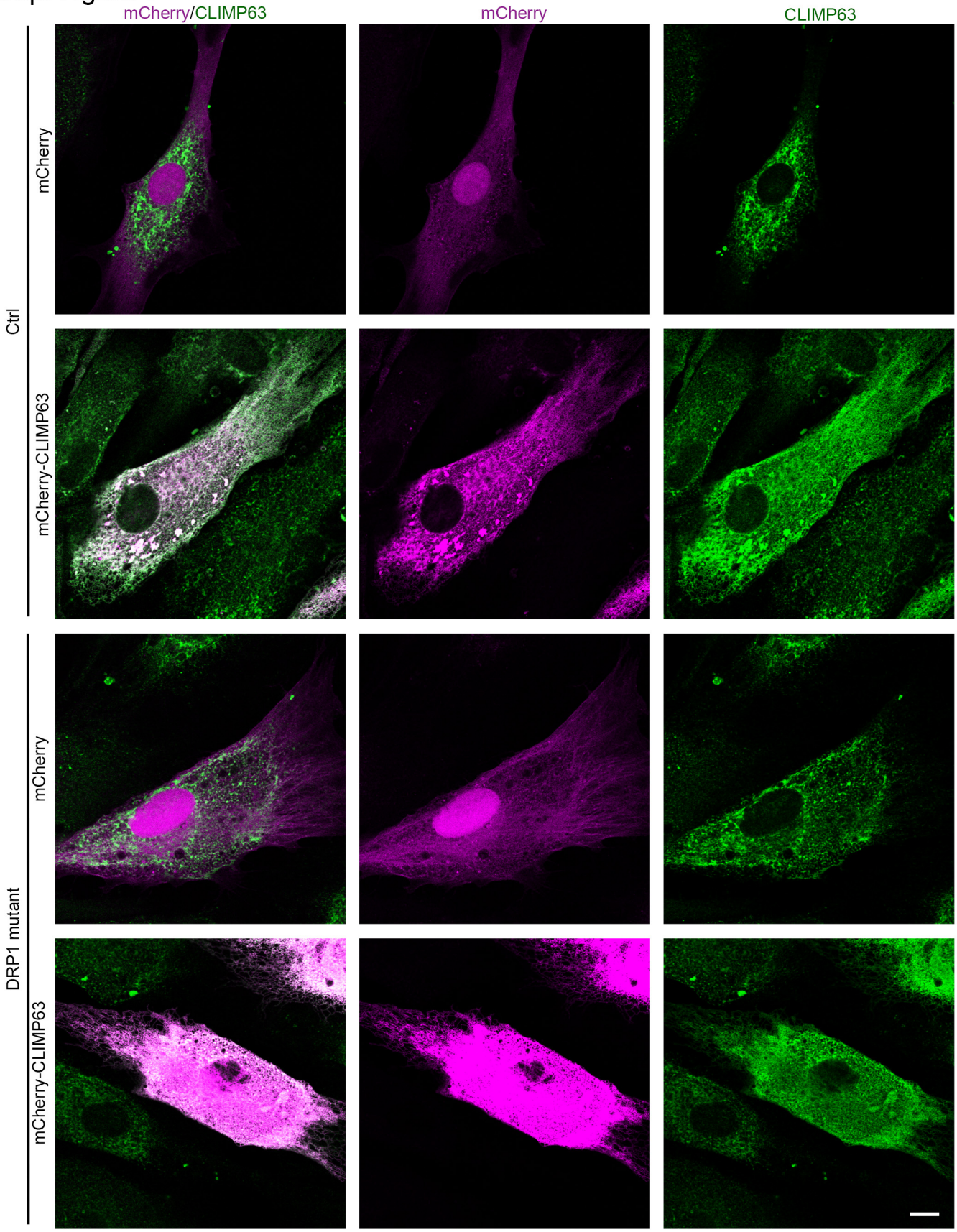
mCherry/CLIMP63
mCherry
CLIMP63
Ctrl
mCherry
mCherry-CLIMP63
DRP1 mutant
mCherry
mCherry-CLIMP63

Sup. Figure 5

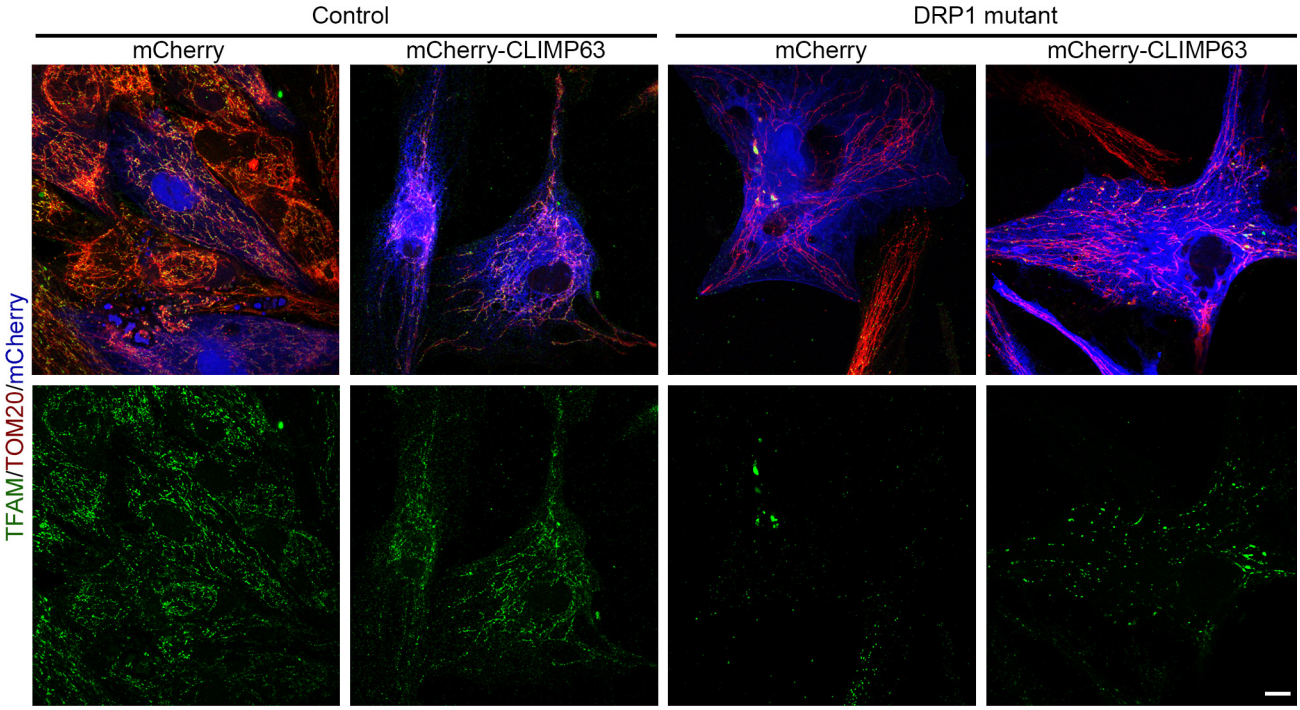
Control
DRP1 mutant
mCherry
mCherry-CLIMP63
mCherry
mCherry-CLIMP63
TFAM/TOM20/mCherry